

# Magnetic chitosan nanocomposite: Fabrication, properties, and optimization for adsorptive removal of crystal violet from aqueous solutions

Mohamadreza Massoudinejad<sup>a</sup>, Hassan Rasoulzadeh<sup>b,\*</sup>, Mansour Ghaderpoori<sup>c,d</sup>

<sup>a</sup> Department of Environmental Health Engineering, School of Public Health and safety, Shahid Beheshti University of Medical Sciences, Tehran, Iran

<sup>b</sup> Department of Environmental Health Engineering, Student Research Committee, Faculty of Public Health and safety, Shahid Beheshti University of Medical Sciences, Tehran, Iran

<sup>c</sup> Department of Environmental Health Engineering, School of Health and Nutrition, Lorestan University of Medical Sciences, Khorramabad, Iran

<sup>d</sup> Nutritional Health Research Center, Lorestan University of Medical Sciences, Khorramabad, Iran

## ARTICLE INFO

### Keywords:

Chitosan  
Crystal violet  
Kinetic  
Nanocomposites  
Recovery

## ABSTRACT

Recovery of crystal violet (CV) dye was investigated using magnetic chitosan nano-composites (MCNCs) and the effects of process variables (contact time, initial CV concentration, adsorbent dose, and pH) were optimized through response surface methodology. The reliability of the RSM models (first-order model, first model with interaction, the second-order model, and reduced model) was tested by fitting the data. A comparative analysis of the results derived from the models demonstrated that the reduced model was the best. According to modelling results, MCNCs dosage and contact time were found to be the most effective variables on the adsorption efficiency procedure, respectively. Also, pH had no significant effect on the adsorption uptake statistically. MCNC has the maximum adsorption efficiency (72%) when the contact time, adsorbent dosage, and initial concentration of CV were optimally set as 140 min, 1 g, and 77 mg/L, respectively. Quantity uptake of CV was evaluated using the Langmuir, Freundlich, and Temkin models. Based on findings, Freundlich isotherm fitted well with the experimental results. Kinetic studies showed that the pseudo-first-order model fitted the best the experimental data, which indicated that the adsorption rate of CV molecules onto MCNC was time-dependent. The studies on the well regenerability of MCNC in addition to its high potentiality of cationic dyes removal make it an attractive adsorbent in terms of dye-containing wastewaters treatment.

## 1. Introduction

Water pollution has become a serious environmental problem and has attracted global concern in recent years (Pandey & Mishra, 2014; Pandey & Ramontja, 2016; Pandey, 2017). Pollutants that are of primary concern include metals, dyes, biodegradable waste, phosphates and nitrates, hazardous and toxic chemicals, radioactive pollutants, pharmaceuticals, and personal care products (Makhado, Pandey, Nomngongo, & Ramontja, 2018; Makhado, Pandey, & Ramontja, 2018). Dyes are a big part of these hazardous materials. Among the dyes, Crystal Violet (CV) belongs to the group of basic dyes. It is one of the most important cationic dyes (Loqman, El Bali, Lützenkirchen, Weidler, & Kherbeche, 2016), and categorizes as a recalcitrant molecule (Muthukumaran, Sivakumar, & Thirumarimurugan, 2016). The CV is widely used in the production of printing inks, in many industrial fields like leather, paper-making, food, cosmetic and textile industries, biological stain, and as a dermatological agent (Loqman et al., 2016). It is

toxic to mammalian cells and also a mutagen, mitotic poison, a proven potent carcinogen (Elwakeel, El-Bindary, El-Sonbati, & Hawas, 2017), allergic dermatitis (Loqman et al., 2016), nausea, vomiting, profuse sweating, and mental confusion while ingestion through mouth (Rafatullah, Sulaiman, Hashim, & Ahmad, 2010). Also, it can cause permanent injury to the cornea and conjunctiva (Elwakeel, El-Bindary, El-Sonbati, & Hawas, 2017). Therefore, it is highly important to treat the wastewater containing CV for environmental safety, human's health as well to safeguard the living biota.

Several methods have been applied to clean of dye-bearing effluents, namely biological treatment (Morshedi, Mohammadi, Boojar, & Aliakbari, 2013). This methods include physicochemical treatments (Qian, Sun, & Liu, 2013), oxidation (Cao, Luo, Lin, Xu, & Chen, 2012), coagulation (Morshedi et al., 2013), membrane filtration (Kurt, Koseoglu-Imer, Dizge, Chellam, & Koyuncu, 2012), and adsorption (Dotto et al., 2017). Each of these processes aforementioned faces certain merits and limitations. However, the adsorption due to its

\* Corresponding author.

E-mail addresses: [Hasanseng@gmail.com](mailto:Hasanseng@gmail.com), [Hrasoulzadeh@sbmu.ac.ir](mailto:Hrasoulzadeh@sbmu.ac.ir) (H. Rasoulzadeh).

<https://doi.org/10.1016/j.carbpol.2018.11.048>

Received 14 September 2018; Received in revised form 2 November 2018; Accepted 16 November 2018

Available online 19 November 2018

0144-8617/ © 2018 Elsevier Ltd. All rights reserved.

merits of simplicity, ease of operation, possibility of regeneration, cost-effective, high efficiency, and capability for adsorption a wide range of dyes. This process is superior amongst all the treatment techniques (Tahir, Bhatti, Iqbal, & Noreen, 2017). Application of activated carbon as a main adsorbent has been found to have higher adsorption capacity for its high surface area in dye removal but it is very expensive. Thus, the reusable and low-cost alternative has been the focus of recent research. It is well known that biomaterials can be obtained and used for environmental remediation objectives (Loqman et al., 2016). Recently, some studies have been assessed the dyes adsorption by such materials in aqueous solutions. As an example, Chen et al. investigated the method of removing food yellow 3 from synthetic solutions by chitosan grafted adsorbing on poly (quaternary ammonium)/Fe<sub>3</sub>O<sub>4</sub> nanoparticles (Yu et al., 2016). Elwakeel et al determined the basic dyes such as crystal violet removal potential from aqueous solutions by adsorption on magnetic alginate beads (Elwakeel, El-Bindary et al. 2017). Chitosan is one of the most widely studied biopolymers for recovery of contaminants from aqueous solutions. It is biocompatibility, recyclability, biodegradability, hydrophilicity, and polyelectrolyte properties. It is a natural polysaccharide prepared from chitin which has been found in different natural sources like annelids, crustaceans, mollusks, annelids, insects, fungi, and coelenterata (Yu et al., 2016). Chitosan consists of two hydroxyl groups and one amino group in each repeating monomer. The presence of nitrogen heteroatoms can enhance CV adsorption on this adsorbent (Vakili et al., 2014). It has very affinity adsorption for dyes and some metal ions. However, the main barriers to the use of raw chitosan as the adsorbent include the poor mechanical strength, low-surface area, and low thermal resistance as well it's very hard to be separated by traditional separation methods (Yu et al., 2016).

To solve this issue, the researchers used modified chitosan to prepare different derivatives such as magnetic nanoparticles (Yu et al., 2016). The coating of magnetite nanoparticles onto chitosan is a promising method to overcome this obstacle encapsulation of magnetite within a chitosan matrix upgrades its mechanical strength and regeneration ability (Reddy & Lee, 2013).

The aim of this study was the use of magnetic chitosan nanocomposites (MCNCs) for adsorption of CV under optimum conditions (including contact time, initial dye concentration, adsorbent dose, and pH) from aqueous solutions utilizing the response surface methodology (RSM) based on Central-Composite statistical design (CCD). The RSM is an empiric statistical technique. It has been used to analyze the effect of main factors to determine operating conditions and regression model (Massoudinejad et al., 2018). Moreover, the isotherm modelling, kinetics, and thermodynamic parameters were investigated.

## 2. Materials and methods

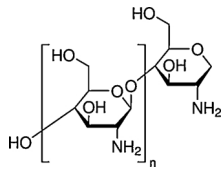
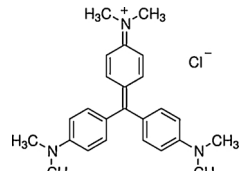
### 2.1. Chemical and reagents

Chemicals of ethanol, epichlorohydrin, and acetic acid were purchased from Merck Co. Also, FeCl<sub>3</sub>·6H<sub>2</sub>O, FeSO<sub>4</sub>·7H<sub>2</sub>O, ammonium hydroxide (purity: 25%), medium molecular weight chitosan (CAS Number: 9012-76-4, Molecular Weight 10<sup>5</sup> g/mol), and CV dye (C<sub>25</sub>H<sub>30</sub>N<sub>3</sub>Cl, λ<sub>max</sub> = 584 nm) were purchased from Sigma-Aldrich Co. The structure and properties of chitosan and CV were shown in Table 1. The stock solution of CV (1000 ppm) was prepared in deionized water and further diluted to achieve the needed concentrations (based on C<sub>1</sub>V<sub>1</sub> = C<sub>2</sub>V<sub>2</sub>). All materials were of guaranteed or analytical grade and used without further purification.

### 2.2. Fabrication of magnetic (Fe<sub>3</sub>O<sub>4</sub>) chitosan nanocomposites (MCNCs)

The Fe<sub>3</sub>O<sub>4</sub> nanoparticles were fabricated according to the study carried out by previous researchers (Zulfikar, Afrita, Wahyuningrum, & Ledyastuti, 2016). Nanoparticles were prepared via co-precipitation

**Table 1**  
Structure and properties of chitosan and CV used in this work.

Chitosan		Crystal violet (CV)		
Molar mass	CAS Registry no	Molecular formula	Molar mass	CAS Registry no
10 <sup>5</sup> g mol <sup>-1</sup>	9012-76-4	C <sub>25</sub> H <sub>30</sub> N <sub>3</sub> Cl	408 g mol <sup>-1</sup>	548-62-9
Structure		Structure		
				

method, in which FeSO<sub>4</sub>·7H<sub>2</sub>O (0.023 mol) and FeCl<sub>3</sub>·6H<sub>2</sub>O (0.046 mol) was added into 150 mL distilled water under N<sub>2</sub> atmosphere for 3 min in 250 mL three-necked flask. Then, 20 mL ammonia solution (25%) was added quickly into the mixed solution under vigorous stirring. After 30 min, to modify nanoparticles in the mixture, 3 mL epichlorohydrin was added to the solution and heated to 75 °C for 1 h under continuous N<sub>2</sub>. After that, it cooled to room temperature. Finally, the nanoparticles obtained were collected through magnetic separation and washed three times with deionized water and ethanol. After synthesis, final product dried in vacuum oven.

For the preparation of MCNCs, Chitosan (0.5 g) was dissolved in 100 mL of acetic acid. Crosslinking was achieved at 65 °C and pH 6 by adding 1.5 g modified Fe<sub>3</sub>O<sub>4</sub> nanoparticles into a three-necked flask for 4 h mixture refluxing. After the reaction, the powders obtained were collected through magnetic separation and washed three times with deionized water and ethanol, respectively. Final MCNCs dried in vacuum oven.

### 2.3. Apparatuses and techniques in experiments and adsorbent characterization

Solutions pH were observed by WTW inoLab pH 720 pH meter. A magnetic stirrer model IKA® C-MAG HS 7 (USA), was used for the mixing of the solutions. Samples agitation were done using orbital shaking incubator model (HOLDER 5000D Orbital motion). An electronic balance model Kern, ABJ 220-4NM was used to measuring the weights of the adsorbent. The concentration of CV measurements was performed by Hach LPG408.99.00012 Dr5000 Uv-vis Spectrophotometer (Germany), at λ<sub>max</sub> = 584 nm. Scanning electron microscope (SEM); JSM-7100FA and X-ray diffractometer (XRD) Quanta Chrome, NOVA, 2000 were applied to study the morphology of NCs. The particle size of MCNCs was observed by using Transmission Electron Microscope (TEM). XPS was performed using an AXIS HSi spectrometer. The method of Brunauer-Emmett-Teller (BET) by N<sub>2</sub>-adsorption in a Micromeritics Instrument Crop, GA, was applied to analyze the pore size distribution and surface area of MC nanocomposites. A Bruke EQUINOX 55 (Germany) Fourier transform infrared (FT-IR) spectrometer was utilized to investigate the chemical structure of synthesized NCs. The zero point charge (pH<sub>zpc</sub>) of the Fe<sub>3</sub>O<sub>4</sub> and MC nanocomposites were recorded using a Malvern ZEN2600 Zetasizer Nano Z.

### 2.4. Crystal violet (CV) batch adsorption experiments

The adsorption of CV on MCNCs was evaluated by batch experiments. Input variables were initial CV concentration (5–100 mg/L), MCNCs dosage (0.02–1 g/L), solution pH (2–12), and the contact time

(5–200 min). To carry out the adsorption experiments, at first 100 ml of each concentration was taken in an Erlenmeyer flask and purpose dosage was added. Then, HCl and NaOH (0.1 N) was used to adjust solution pH. Finally, the samples were mixed in a thermostated stirrer. Additionally, after the desired shaking time, the loaded adsorbent was recovered by separation using the external magnetic field (1.4 T). Moreover, In order to improve the accuracy of the experiments, the supernatant was filtrated and residual CV concentration was determined by a Spectrophotometer (DR-5000). All experiments were performed at room temperature and the mixing rate of 200 rpm.

In this work, the adsorption Kinetic, isotherm and thermodynamic studies were performed. based on the CCD method, under the different experimental condition, the removal efficiency of CV was obtained. Finally, to obtain CV adsorption (mg/g) on MCNCs and its removal percentage, the following relationship (Eqs. (1) and (2)) was used (Yilmaz, Şahan, & Karabakan, 2017):

$$q_e = \frac{(C_0 - C_e)V}{M} \quad (1)$$

$$R, \% = \frac{C_0 - C_e}{C_0} * 100 \quad (2)$$

Where,  $q_e$  is the equilibrium adsorption(mg/g).  $C_0$  and  $C_e$  are the CV concentration at the initial and equilibrium in solution (mg/L), respectively.  $V$  and  $M$  are the volume of studied solution (L) and the mass of MCNCs for each solution (g), respectively.

### 2.5. Statistical analyses and optimization by using the CCD approach

To obtain the optimum conditions for the adsorption of CV on the MCNCs, RSM based on CCD was used as a useful statistical technique (Van Thuan, Quynh, Nguyen, & Bach, 2017). In this study, RSM approach was utilized to determine the main effect (including initial concentration, adsorbent dosage, pH of the solution, and the contact time), reciprocal interaction between them toward one output response (CV removal efficiency), and determining optimal conditions (Van Tran, Bui, Nguyen, & Bach, 2017). The parameters considered for the modelling study were being coded at three levels (-1, 0, +1) as shown in Table 2.

According to CCD design, the total of 44 runs (by using equation  $2^k + 2k + C$ ) were carried out to evaluate the CV adsorption on MCNCs. In the formula,  $k$ ,  $C$ ,  $2^k$ , and  $2k$  represents the number of central points, the number of independent parameters, factorial experiments, and axial experiments, respectively. At centre point, 20 replications were used to determine experimental error (Ayazi, Khoshhesab, Azhar, & Mohajeri, 2017; Massoudinejad, Ghaderpoori, Shahsavani, & Amini, 2016). To obtain an appropriate response-surface model, the attained data were analyzed by RSM models. The models included FO, FOI, and SO depicts a first-order model, the first model with interaction and second-order model, respectively. Additionally, reduce model was used if was required. Also, to optimization studies and further analysis, the best model was selected. In this process (selection of best model), four parameters were considered. The model with the higher  $R^2$ , the smaller  $p_{value}$ , more lack of fit (or insignificant lack of fit), and greater  $F_{value}$  was selected as the suitable model (Massoudinejad et al., 2016). The

**Table 2**

Actual values of independent variables used for experimental design.

Variable	Symbol	-1	Coded	
			0	1
			level	
			Real values	
Initial CV concentration (mg/L)	$X_1$	5	102.5	100
pH of the solution	$X_2$	2	7	12
Contact time (min)	$X_3$	5	102.5	200
Adsorbent (g/L)	$X_4$	0.02	0.51	1

optimized conditions for the response value CV molecules removal that is correlated to the independent variables were approximated using the following empirical second-order polynomial model Eq. (3)(Gupta, Agarwal, Asif, Fakhri, & Sadeghi, 2017):

$$Y = b_0 + \sum_{i=1}^k b_i X_i + \sum_{i=1}^k b_{ii} X_i^2 + \sum_{i=1}^{k-1} \sum_{j=1}^k b_{ij} X_i X_j + C \quad (3)$$

Where,  $Y$  is the contaminant removal (%) percentage (predicted response).  $x_i$  and  $x_j$  are the parameters being studied. The  $b_0$  is the regression coefficients for intercept, and  $b_i$ ,  $b_{ii}$ , and  $b_{ij}$  are the linear, quadratic, and interaction effects, respectively. Also,  $C$  is the error of prediction.

The analysis of variance, ANOVA, was utilized to obtain the significance level of the variables. Moreover, the Solver Add-ins were utilized to determine the optimum conditions, using significant parameters to prepare a mathematical model as predicted by RSM (Bandpei et al., 2017). All analyses were carried out using R software version 3.0.3.

## 3. Results and discussion

### 3.1. Characterization results

Detailed information about the MC was obtained by FTIR, SEM, XPS, TEM, XRD, and BET. To better understand the concept of stabilization mechanisms, FTIR analysis was conducted to identify possible interactions between chitosan and  $Fe_3O_4$  molecules. In addition, FTIR spectroscopy is a powerful, well-developed method to determine the structure and identification of chemical species. It is mainly used to identify organic compounds because of the complexity of their spectra. The FTIR spectra of Chitosan, MC and  $Fe_3O_4$  are shown in Fig. 1. It's shown that some obvious changes take place in the spectrum of MCNCs in comparison with the pristine chitosan spectrum and bare  $Fe_3O_4$ . The IR spectrum of chitosan was characterized as follows ( $cm^{-1}$ ): a strong and broad absorption band at 3421 (O–H and amino groups); a weak bands at 2885 (antisymmetric and symmetric aliphatic C–H); a middle strong bands at 1647 and 1597 (deformation of C=O stretching vibration of amide and the bending vibration of  $-NH_2$  groups, respectively); 1423 and 1379 (C–CH<sub>3</sub>); 1251 (amide III), and 1095 (skeletal vibration of C–O stretch) (Geng, Jin, Li, & Qi, 2009). The FTIR spectrum for MC nano-composites (Fig. 1) showed several shifts in wave-numbers of new peaks. On the other hand, the appeared signals at 576 and 422 (Fe–O bands in tetrahedral and octahedral sites) indicated that the MC nano-composites were successfully coated with chitosan (Zulfikar, Afrita, Wahyuningrum, & Ledyastuti, 2016).

To show the structure of the chitosan-coated magnetic  $Fe_3O_4$  nanocomposites, the morphology of MC was investigated by SEM images. The results showed sphericity and an almost uniform distribution of synthesized nanoparticles (Fig. 2a). Fig. 2b shows that, after using chitosan as a stabilizer, the surface of the magnetic  $Fe_3O_4$  was covered by chitosan.

The surface area of  $Fe_3O_4$  and MC nano-composites were found to be 98.6 and 88.7  $m^2/g$ , respectively by  $N_2$  adsorption isotherms. So, this decreasing of surface area can be due to the tight cumulated structure. Also, pore diameters of all adsorbents were in the range of 5–50 nm; which revealed the mesoporous nature of the MC nano-composites (Ahmadi, Niari, & Kakavandi, 2017). To understand the surface chemical composition of the functionalized MC nano-composites, XPS characterization was employed. Fig. 3 shows the full XPS patterns, in which the binding energies relating to Fe 2p<sub>3/2</sub> and Fe 2p<sub>1/2</sub> were 711.0 and 724.3 eV, respectively. These binding energies data are close to the previous data of  $Fe_3O_4$  in the literature (He et al., 2010).

The size and morphology of nanoparticles observed by TEM showed that the magnetic nanoparticles have good uniformity and high crystallization (Fig. S1 of supplementary data). XRD was used to determine

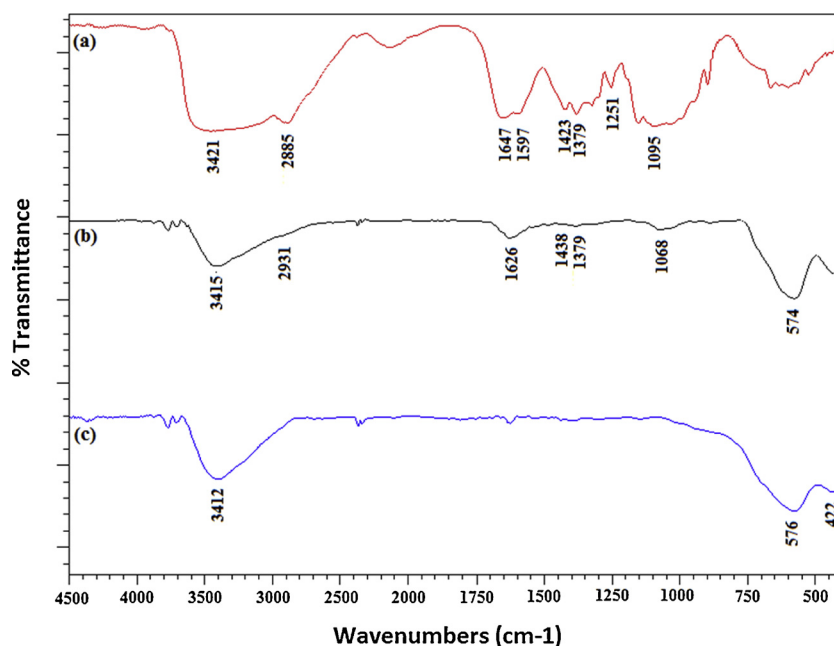


Fig. 1. FTIR spectra for Chitosan (a), MC (b), and Fe<sub>3</sub>O<sub>4</sub> (c).

the crystal and spectral structures of the MC (Fig. 4). According to the peak patterns of MC obtained by XRD analysis ( $2\theta = 220, 311, 400, 422, 440,$  and  $511$ ), the presence of the chitosan biopolymer caused no changes in the Fe<sub>3</sub>O<sub>4</sub> core. Also, the presence of Fe<sub>3</sub>O<sub>4</sub> crystals was confirmed by comparing the recorded peaks with standard peaks.

The zeta potentials of the Fe<sub>3</sub>O<sub>4</sub> and MC nano-composites (0.1 mg/mL) were measured in 50 ml of NaCl ( $10^{-3}$  M) at initial pH 2 to 12. As shown in Fig. 5,  $pH_{zpc}$  of the Fe<sub>3</sub>O<sub>4</sub> nanoparticles was about 7.1, which consistent with the literature value of 6.7 (Chang & Chen, 2005). After chitosan bonding, the  $pH_{zpc}$  was shifted to 6.5. This, also, confirms the coating of chitosan and evident that the MC nano-composites were positively charged at  $pH < 6.5$ .

### 3.2. Fitting a response-surface model and developing a regression model equation

Based on CCD, the complete design of experiments and responses are presented in Table S1 (in the Supplementary data). The aforementioned RSM models were tested by fitting the data in terms of the reliability. Specification of the response-surface portion of each model was performed based on particular information such as  $p_{value}$ ,  $F_{statistic}$ , multiple R-squared, adjusted R-squared, and lack of fit (Murugesan et al., 2014). The results of modelling with different models are recorded in Table S2 (in the Supplementary data).

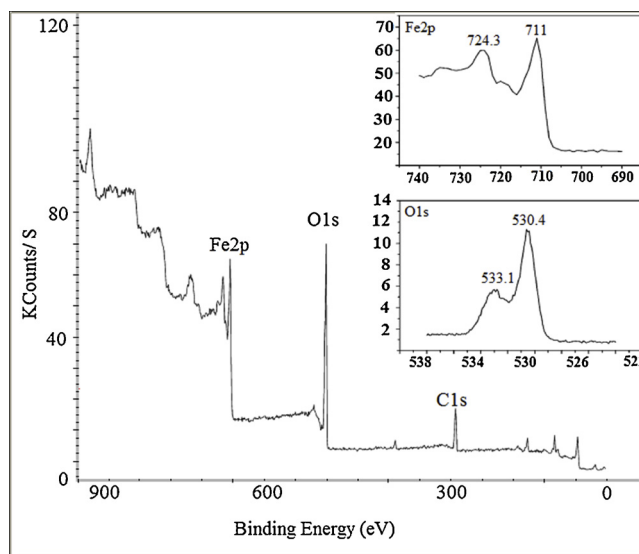


Fig. 3. XPS spectra of MC nano-composite (the expanded spectra are for Fe 2p and O 1 s).

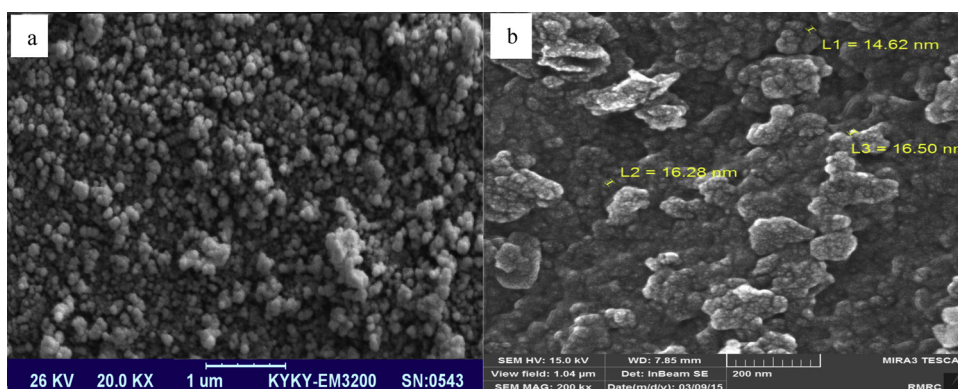


Fig. 2. SEM images of Fe<sub>3</sub>O<sub>4</sub> (a) and chitosan-coated magnetic nano-composites (b).

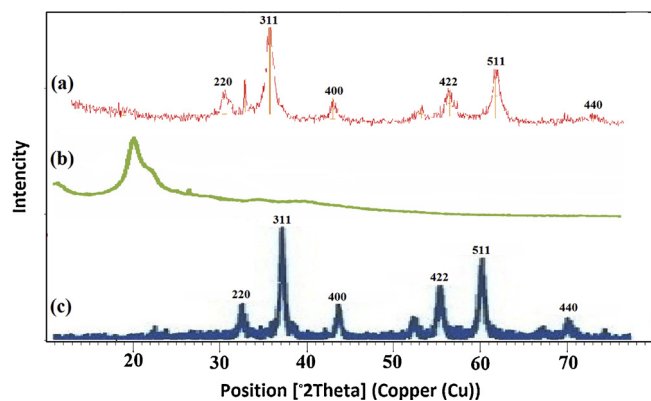


Fig. 4. XRD spectra of  $\text{Fe}_3\text{O}_4$  (a), Chitosan (b), and MC (c) nano-composites.

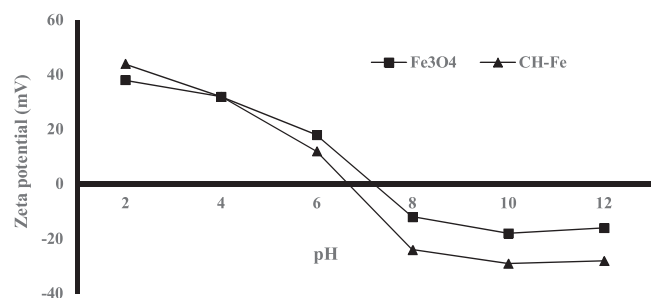


Fig. 5. Zeta potentials of  $\text{Fe}_3\text{O}_4$  and MC at different pH values.

As a determining factor, the lack of fit value, which must be insignificant in the most appropriate model, was checked for all models, and for all of them, it was insignificant (Podstawczyk, Wittek-Krowiak, Dawiec, & Bhatnagar, 2015). Based on the results obtained from the models assert that the reduced model could be the best model. The magnitude of  $F_{\text{value}}$ , highest  $R^2$ , and the smallness of  $p_{\text{value}}$  in addition to the low lack of fit affirm that the corresponding model is the best one. Therefore, the insignificant terms ( $x_2$ ,  $x_1$ ;  $x_2$ ,  $x_1$ ;  $x_3$ ,  $x_1$ ;  $x_4$ ,  $x_2$ ;  $x_3$ ,  $x_2$ ;  $x_4$ ,  $x_3$ ;  $x_4$ ,  $x_2^2$ ,  $x_4^2$ ) are excluded from the quadratic equation, and the reduced full second-order model was obtained. The adequacy of the selected model was evaluated by ANOVA (Subramaniam & Ponnusamy, 2015).

Considering Table S3, in the supplementary data,  $F_{\text{value}}$ ,  $p_{\text{value}}$ ,  $R^2$ , and lack of fit further verified the adequacy of the reduced model (Sohbatzadeh, Keshkar, Safdari, & Fatemi, 2016). A lower  $p_{\text{value}}$  ( $p < 0.05$ ) and higher  $F_{\text{value}}$  of the model and each variable term in the model indicate a more significant influence of the model and/or terms. The statistical analysis of models ( $F_{\text{value}}$ , 22.71 on 5 and 38 DF;  $p_{\text{value}}$ ,  $< 0.05$ ;  $R^2$ , 0.75, and lack of fit,  $> 0.05$ ) revealed that the reduced full second-order model was the best model for the CV adsorption. As clearly seen in Fig. S2, in the supplementary data, the reduced model provides satisfactory agreement with the experimental data and high correlation coefficient (0.74) is also reaffirming the high adequacy of this model (Chang, Song, Wang, Li, & Ma, 2012).

In a valid statistical model, the values of multiple R-squared and adjusted R-squared must be close to each other; Because with the reduction of the difference between them, the chance of entering non-significant terms into the model is greatly reduced (Subramaniam & Ponnusamy, 2015). In the study, the closeness of multiple R-squared values (0.75) to the adjusted R-squared value (0.72) indicated a good chance for significant terms to be included in the model. Therefore, the model can use for prediction and optimization. The results obtained for the reduced model are reported in Table S4, in the supplementary data.

Accordingly, the significant coefficients ( $x_1$ ,  $x_3$ ,  $x_4$ ,  $x_1^2$ , and  $x_3^2$ ) were retained to enter into the model formulation. The obtained regression equation between the removal of CV (Y) and the coded

variables as given below (Eq. (4)):

$$Y = 66.09 - 0.308X_1 + 0.14X_3 + 7.46X_4 + 0.002X_1^2 + 0.0005X_3^2 \quad (4)$$

Notice that the variables with negative signs ( $x_1$  and  $x_3^2$ ) have an antagonistic effect in adsorption of CV, whereas the variables with positive signs ( $x_3$ ,  $x_4$  and  $x_1^2$ ) show the positive relationship and have a synergistic effect on the removal efficiency and also in predicting the model response.

### 3.3. Response surface methodology and contour plotting

To optimize the independent variables, two-dimensional (2D) contour and the 3D reaction surface plots were constructed. The effects of contact time (5–200 min) and adsorbent dosage (0.02–1 g/L) were simultaneously monitored for the removal of CV from synthetic wastewater samples. Fig. S3(a, b) of Supplementary data exhibits the effects of the interaction between contact time and adsorbent dosage on the removal capacity in initial CV concentration (52.5 mg/L). It was clear from Fig. S3 when the adsorbent dosage increased, even with shorter/fewer times the removal efficiency increased. This underscores that the effect of dosage, especially in higher times, is very significant. When the adsorbent dosage was 0.5 g/L, the removal efficiency was achieved to be 68%, with a contact time of 102 min. In the adsorbent dosage over 0.75 g/L, even with shorter/fewer contact times (54 min), 70% removal was achieved. The fast removal in the initial stages can be related to the greater concentration gradient and abundance of surface sites on the MCNCs that gradually and occupying the binding sites, decreases with the passage of time (Tahir et al., 2017). It can be concluded that 140 min of contact time was enough for achieving over 70% removal efficiency with 1 g/L of adsorbent.

The correlation of initial CV concentration and adsorbent dosage on the removal uptake is shown in Fig. S4 (a, b), in the Supplementary data. As presented in Fig. S4, both the lower concentrations of CV and higher values of adsorbent dosage increased the removal percentage for CV molecules while the excellent efficiency occurs at 1 g/L of MCNCs and 77 mg/L of CV dye. The enhancement of removal percentage with increasing adsorbent dosage is related to the greater availability of surface area and more adsorptive sites for dye capture (Sarma, Gupta, & Bhattacharyya, 2016). In addition, in low concentrations of CV, higher efficiency was observed, which can be attributed to the high ratio of surface adsorptive sites to dye molecules and saturation of active sites at higher concentrations (Mohammadzadeh, Ramezani, & Ghaedi, 2016).

### 3.4. Process optimization and confirmation

The maximum removal efficiency and optimum conditions corresponding to the CV adsorption on MCNCs were determined by analyzing the experimental data (44 runs) with Solver Add-ins in Microsoft Excel 2013. The optimum conditions for CV concentration (mg/L), contact time (min), and MCNCs dosage (g/L) were found to be 77, 140 and 1, respectively. Under these conditions, the maximum removal efficiency was predicted to be 71.5%. To ensure the adequacy of the model and to affirm the good agreement between the software outputs (predicted maximum removal efficiency) and experimental results, five same runs were performed at the aforementioned conditions. The experimental results revealed an average CV removal efficiency of  $72 \pm 1\%$ . The closeness of predicted maximum removal efficiency (71.5%) to experimental ( $72 \pm 1\%$ ), with a bias of lower than 2%, indicated that the model predicted by RSM could be considered as accurate and valid. Note that the optimization process is critical to minimize operational costs of wastewater treatment on an industrial scale and ensure efficiency.

### 3.5. Adsorption isotherm studies

The adsorption isotherm models were used to fit and evaluate the equilibrium data corresponding to the adsorption of CV on MCNCs. The adsorption equilibrium data were correlated with conventional isotherm models including Langmuir, Freundlich, and Temkin to study the liquid/solid phase dye molecules distribution, adsorbent affinity and mechanism of the adsorption process. A relatively high the coefficient of determination ( $R^2$ ) value regarding their linear regressions was used to find the best fit model. The Langmuir model deals with the study of complete monolayer adsorption on the homogeneous surface with independent adsorption of adsorbed molecules (Van Thuan, Quynh, Nguyen, & Bach, 2017). Linearized of Langmuir equation represented as (Eq. (5)):

$$\frac{C_e}{q_e} = \frac{1}{q_m b} + \frac{1}{q_m} C_e \quad (5)$$

Where,  $c_e$  (mg/L),  $q_e$  (mg/g),  $q_m$  (mg/g) and  $b$  (L/mg) are the equilibrium concentration of CV, amount of pollutant adsorbed per unit weight of adsorbent, maximum adsorption capacity and energy of adsorption, respectively. The values of  $q_m$  and  $b$  were determined by slope and intercepts of the plot of  $c_e/q_e$  against  $c_e$  as presented in Table 3 and represented in Fig. S5.

The dimensionless equilibrium parameter ( $R_L$ ), also known as the separation factor, is an important characteristic of the Langmuir model. It is indicated whether CV adsorption is unfavourable ( $R_L > 1$ ), linear ( $R_L = 1$ ), favorable ( $0 < R_L < 1$ ), and irreversible ( $R_L = 0$ ) (Bagheri, Ghaedi, Asfaram, Bazrafshan, & Jannesar, 2017).  $R_L$  equation represented as (Eq. (6)):

$$R_L = \frac{1}{[1 + bc_0]} \quad (6)$$

Where,  $C_0$  is the initial concentration of dye (mg/L). The Freundlich model deals with the study of multilayer and uneven adsorption of the adsorbate on the heterogeneous surface with lack of uniform distribution of energy and with the interaction between adsorbed molecules. The linear formula used for the Freundlich model is shown below (Eq. (7))(Alimohammadi, Saeedi, Akbarpour et al., 2017):

$$\log q_e = \log k_f + \frac{1}{n} \log C_e \quad (7)$$

In Eq. (7),  $K_f$  (mg/g) (L/mg) $^{1/n}$  and  $n$  are the Freundlich coefficients related to the adsorption capacity of the adsorbent and adsorption intensity of the adsorbent, respectively.  $1/n$  also known as the heterogeneity factor indicating the favorability of the adsorption process. If  $0.1 < 1/n < 1$ , the adsorption is favourable. Moreover, if  $n < 1$ ,  $n = 1$ , and  $n > 1$  the adsorption is linear, chemical, and physical, respectively. Their values ( $K_f$  and  $n$ ) were evaluated by the plot of  $\log q_e$  versus  $\log c_e$  as given in Table 3 and displayed in Fig. S5.

The Temkin model is employed to investigate the heat of the adsorption (adsorption energy) and adsorbent–adsorbate interactions. This isotherm assumes that the decrease of the adsorption energy of all the molecules in a layer linearly with the monolayer sorption on the active sites as a result of adsorbent–adsorbate interactions. The linear form of the Temkin model is given as follows (Eq. (8)) (Dastkhooon et al., 2017):

$$q_e = B_1 \ln(k_t) + B_1 \ln(C_e) \quad (8)$$

**Table 3**  
Langmuir, Freundlich, and Temkin isotherm parameters for the CV adsorption by MCNCs.

$R^2$	Langmuir isotherm			$R^2$	Freundlich isotherm			$R^2$	Temkin isotherm	
	$b$ (L/mg)	$R_L$	$q_m$ (mg/g)		$n$	$1/n$	$K_f$		$k_t$ (L/mg)	$b_1$
0.952	0.0002	0.976	333.33	0.991	1.35	0.74	14.07	0.836	0.41	127.7

Where,  $B_1, B_1 = RT/b_1$ , denotes the Temkin constant (J/mol).  $R$  is the universal gas constant and equal to 8.314 J/mol.  $K$ .  $T$  is the absolute temperature (°K).  $k_t$  and  $b_1$  represent the equilibrium binding constant (L/g) and adsorption heat (kJ/mol), respectively. A plot of  $q_e$  against  $\ln c_e$  was plotted to determine the Temkin isotherm parameters. It's constants presented in Table 3 and shown in Fig. S5, in the Supplementary data.

It was found that the Freundlich isotherm model could be the best model for the description of the adsorption behaviour of CV on the MCNCs with higher regression coefficient ( $R^2 = 0.99$ ). this result indicated the uneven adsorption of the CV on the surface of MCNCs and lack of uniform distribution of active sites on the adsorbent surface (Asfaram, Ghaedi, Yousefi, & Dastkhooon, 2016). In the previously conducted studies, a similar model for the adsorption of CV onto various adsorbents was recorded (Muthukumaran et al., 2016). The maximum monolayer adsorption capacity ( $q_{max}$ ) for CV onto MCNCs was found to be 333.33 mg/g, which indicated that the MCNCs can be used as a potential adsorbent to the removal of CV and other basic dyes. The comparison of  $q_{max}$  of MC for CV removal with the other similar nanomaterial sorbents under similar experimental conditions is shown in Table 4. The separation factor,  $R_L$ , was obtained to be 0.97 for the initial CV concentration of 100 mg/L. Because  $R_L$  was within the range of 0–1 indicated that the CV adsorption on MC is favorable. The value of  $1/n$  in the range of 0.1–1 strongly supports the favorability of adsorption reaction (Asfaram, Ghaedi, Hajati, Goudarzi, & Dil, 2017). The magnitude of  $b_1$  value showed that the fast removal of CV at the initial stage and the smallness of  $k_t$  value implied the weak bonding of CV molecules onto the composite.

### 3.6. Adsorption kinetics studies

The Adsorption kinetics seems to be the most important characteristic in the adsorption process. The kinetic models were employed to express the behaviour of adsorption reaction and mechanism of interaction of MC and CV (Ahmad & Hasan, 2016). The kinetic experiments were performed in contact time range 5–200 min with other optimum conditions such as initial CV concentration (20, 50, or 80 mg/L), dosage (1 g/L), and pH 7 at room temperature.

In the present research, pseudo-first-order (PFO), pseudo-second-order (PSO), and intraparticle diffusion (IPD) models were applied to model the adsorption kinetics data. Higher  $R^2$  values and the closeness of value to 1 in addition to the high agreement between  $q_e$  (experimental) and  $q_e$  (calculated) affirm that the corresponding model is the most appropriate one (Ayazi et al., 2017). The PFO model together with the PSO model evaluates the reaction between solid and liquid phases. The linear equation of PFO model is (Eq. (9)) (Saleh, Sari, & Tuzen, 2017):

$$\log q_e - q_t = \log q_e - \frac{k_1}{2.303} t \quad (9)$$

where,  $q_e$  and  $q_t$  is the amount of pollutant adsorbed on an adsorbent (mg/g) at equilibrium and time  $t$  (min), respectively. The  $k_1$  is related to the PFO rate constant (1/min). Values of  $k_1$  and  $q_e$  can be obtained by slope and intercepts of the plot of  $\log (q_e - q_t)$  vs  $t$  as presented in Table 9.

The PSO model was used to predict kinetics of chemical sorption as a rate-controlling step. The linear formula used for this model is shown

**Table 4**  
Comparison of CV adsorption with different adsorbents.

Adsorbent	q <sub>m</sub> (mg/g)	Refs.
Montmorillonite (Mt)	370.37	(Sarma et al., 2016)
SnFe2O4@activated carbon magnetic cellulose	158.73	(Rai, Gautam, Banerjee, Rawat, & Chattopadhyaya, 2015)
sugarcane bagasse modified with Meldrum's acid (SMA)	118.9 – 304.9	(Zhou et al., 2014)
SDS coated maghemite nanoparticles	692.1	(Ferreira et al., 2015)
nanoscale zero-valent iron Sargassum swartzii (nZVI-SS) biocomposite	166.7	(Muthukumar, Sivakumar et al. 2016)
SiO2@MgO composite (SMC)	200.00	(Jerold et al., 2017)
Magnetic Chitosan Nano-composites (MCNCs)	2244.85	(Pei, Wang, Tian, Xu, & Yuan, 2015)
	333.33	This study

below (Eq. (10)) (Zulfikar, Afrita, Wahyuningrum, & Ledyastuti, 2016):

$$\frac{t}{q_t} = \frac{1}{k_2 q_e^2} + \frac{1}{q_e} t \tag{10}$$

While, k<sub>2</sub> represents PSO rate constant (g/mg.min). Additionally, the IPD model is conveniently employed to recognize the diffusion mechanism. The model can be epitomized as (Eq. (11)) (Saad, Tahir, Khan, Hameed, & Saud, 2017):

$$q_t = k_{id} \cdot t^{1.2} + C \tag{11}$$

Where, k<sub>id</sub> (mg/g) is related to the IPD rate constant. C is the intercept and represents the thickness of the boundary layer (mg/g), which the effect of this layer depends on the value of the intercept.

The obtained kinetic parameters and constants for all of the models ordered in Table 5 and represented in Fig. S6 (a, b, and c), in the supplementary data. Based on the data obtained, the high R<sup>2</sup> values (in the range of 0.98–0.99), as well as the consistency of theoretical q<sub>e</sub> and experimental q<sub>e</sub> values for the pseudo-first-order model, assert that the adsorption mechanism of CV on MCNCs followed the pseudo-first-order model kinetic. This suggests the adsorption rate of CV molecules on MCNCs is time-dependent, which is due to the presence of abundant surface (and the internal reactive sites) and later, saturation of this sites with time. It was observed that the values of k<sub>1</sub> reduced with increasing dye concentration, which indicated a short time adsorption process occurs to reach equilibrium in lower concentration. Also, the values of k<sub>2</sub> reduced with increasing CV concentration. So, it was concluded that in a lower concentration, the rate of adsorption is higher (Asfaram et al., 2016). Based on the intra-particle diffusion model, the high values of C parameter indicated that the boundary layer effect was also responsible for adsorption. The multi-linearity of q versus t<sup>0.5</sup> plot, and/or deviation of the plots from the origin further confirms that adsorption process is complex and some other mechanisms along with intraparticle diffusion control the process steps, as reported previously by Jerold et al (Jerold, Vasantharaj, Joseph, & Sivasubramanian, 2017). All these indicated that MCNCs has a potential of being used as an adsorbent to remove CV and other cationic dyes from aqueous solutions.

### 3.7. Effect of temperature and thermodynamic studies

The adsorption thermodynamic study in a view of the practical

**Table 5**  
Various parameters of kinetic models for the CV adsorption by MCNCs.

C <sub>0</sub> mg/L	q <sub>e</sub> , Experiment(mg/g)	Pseudo-first order			Pseudo-second order			Intra-particle diffusion		
		R <sup>2</sup>	k <sub>1</sub> (1/min)	q <sub>e</sub> , Calculated (mg/g)	R <sup>2</sup>	k <sub>2</sub> (g/mg. min)	q <sub>e</sub> , Calculated (mg/g)	R <sup>2</sup>	C (mg/g)	K <sub>id</sub> (mg/g. min <sup>1/2</sup> )
20	10.20	0.98	0.014	9.29	0.97	0.0371	8.86	0.95	3.97	3.82
50	22.35	0.99	0.013	25.70	0.97	0.0047	18.34	0.97	11.77	2.98
80	40.22	0.99	0.012	37.83	0.97	0.0028	20.62	0.94	18.69	0.90

CS@nZVI = 1, pH = 7.0, adsorption time = 5–200 min.

application is important because it provides key information about the feasibility, spontaneity, and the thermal nature of the adsorption reaction. To investigate the temperature influence on the removal process, the adsorption experiments were carried out in the temperature range 293–338 °K. With increase in the temperature, the rate of CV diffusion onto the MCNCs and the mobility of the CV molecules increases, confirming that the interaction was an endothermic process (Elwakeel, El-Bindary et al. 2017).

K<sub>D</sub> is defined as adsorption equilibrium constant and was determined with the van't Hoff equation (Eq. (12)), then thermodynamic constants of MCNCs (ΔH°, ΔG°, and ΔS°) were evaluated with conventional thermodynamic equation (Eqs. (13)–(15)):

$$K_D = \frac{q_e}{C_e} \tag{12}$$

Where, q<sub>e</sub> (mg/g) and C<sub>e</sub> (mg/l) denote adsorption capacity of nano-composites and concentration of a pollutant in solution at the equilibrium time, respectively.

$$\Delta G^\circ = -RT \ln K_D \tag{13}$$

$$\Delta G^\circ = \Delta H^\circ - T\Delta S^\circ \tag{14}$$

$$\ln K_D = \frac{\Delta S^\circ}{R} - \frac{\Delta H^\circ}{RT} \tag{15}$$

Where, R is the universal gas constant and equal to 8.314 J/mol. K. T is absolute temperature (°K). ΔG°, ΔH°, and ΔS° are Gibbs free energy change (kJ/mol), standard enthalpy change (kJ/mol), and entropy change (J/mol. K), respectively. After calculating equilibrium constant and related ΔG° at various temperatures, as represented in Table S5 of supplementary data; The values of ΔH° and ΔS° which are slope and intercept of ln K<sub>D</sub> versus 1/T plot were evaluated (Figs. S7 and S8 in the supplementary data).

The negative values of ΔG° confirm the spontaneous nature of the adsorption of CV molecules on the MCNCs. As the temperature of the system increased, the negativity of ΔG° also increased, and proved that the temperature has a synergistic effect on the favorability. The positive value of ΔH° indicates that the adsorption reaction is endothermic. The positive value of ΔS° further confirms that the “disorder” of the system increases as a result of CV adsorption on the surface of MCNCs.

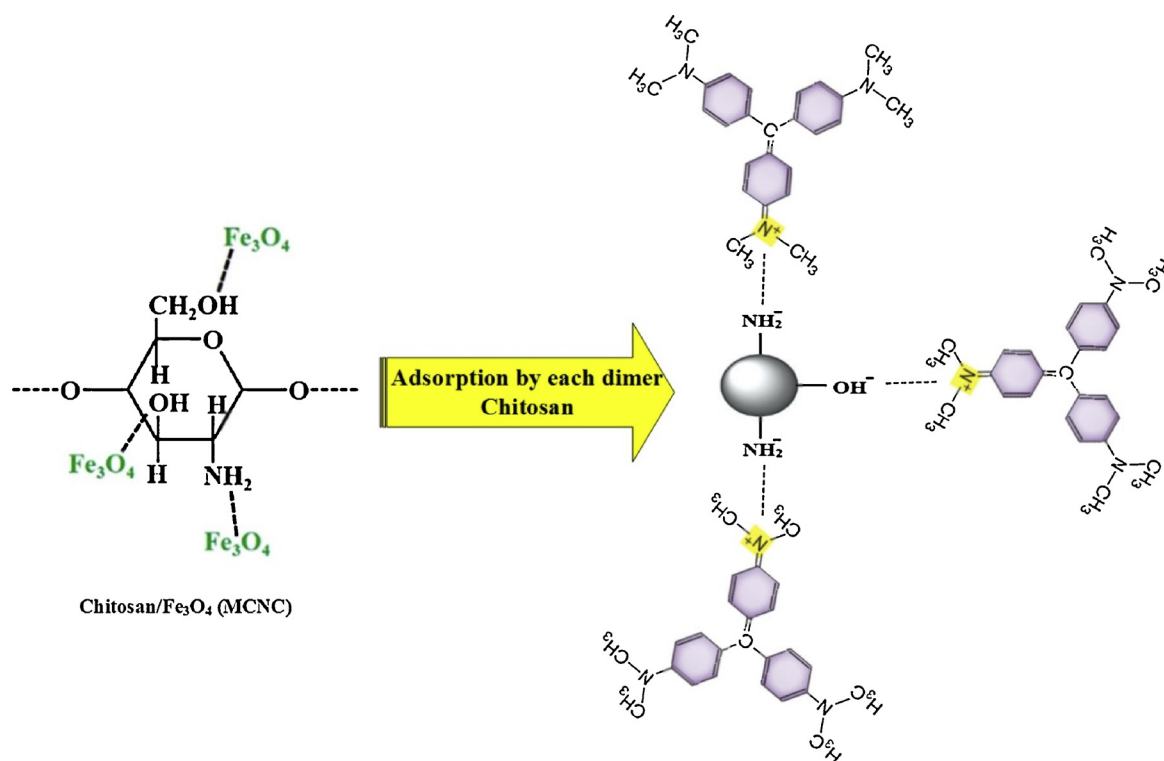


Fig. 6. Schematic representation mechanism for the adsorption of CV on MCNCs.

### 3.8. Recovery and reusability of the composite

Regenerability of adsorption is one of the crucial properties of a typical adsorbent, which this factor was investigated. The original aims of regenerability assessment were to select cost-effective adsorbent and mitigate possible environmental impacts after disposal of that. Adsorption process in the regenerability experiments of CV on the MCNCs was evaluated under the optimum condition. After each adsorption process, the spent adsorbent was magnetically collected and washed with HCl (0.1 M) followed by neutralizing with NaOH (0.1 M) and used for the next adsorption process. The aforementioned cycle was repeated for six series. At the end of each cycle, the regeneration efficiency (%) was determined via the following Eq. (16) (Ahmadi, Foadivanda, Jaafarzade et al., 2017):

$$\text{Regeneration efficiency (\%)} = \left[ \frac{\text{Amount of desorbed}}{\text{Amount of adsorbed}} \right] \times 100 \quad (16)$$

As it is obvious from Fig. S9 in the supplementary data, the regeneration efficiency of the adsorbent was almost stable up to the four cycles. After the fourth cycle, it is sharply reduced. It can be due to leaching of MCNCs by stirring with HCl. From these, MCNCs were found to be a stable adsorbent and can be reused four times with good performance. This confirms a significant balance between its Affordability and its ecological impact.

### 3.9. Mechanism of adsorption

The FTIR analysis showed that the peaks were mainly from the contribution of  $-\text{OH}$  and  $-\text{NH}$  stretching,  $\text{C}-\text{H}$  stretching,  $-\text{NH}$  bending in  $-\text{NH}_2$ ,  $-\text{C}-\text{O}-\text{C}-$  stretching, and  $\text{Fe}-\text{O}$  bond vibration of  $\text{Fe}_3\text{O}_4$ . This revealed that the functional groups such as  $-\text{NH}_2$ ,  $-\text{OH}$ , originally presented in chitosan, were intact after coating on  $\text{Fe}_3\text{O}_4$  and were available for interaction with the dye.

The electrostatic interaction between chitosan and CV can be predicted from the ionic charge of their active sites/functional groups.  $\text{NH}_2$  and  $-\text{OH}$  was chosen as anion adsorption sites of dimer chitosan. On

the other hand, CV has amino cationic groups. The highest difference charge might become the most possible interaction which occurred between adsorbent and adsorbate active sites. Based on Fig. 6, the ligand between the aforementioned oppositely charged groups has the highest difference charge. Therefore, in this case, the most possible interaction ligand between chitosan and CV occurred through the interaction between  $\text{NH}_2$  and  $-\text{OH}$  of chitosan and amino cationic groups of CV. As the adsorption kinetics data justify that the adsorption of CV on MC followed the intra-particle diffusion model, which implies CV adsorption on MCNC was complex and some other mechanisms (such as chemical process/electrostatic interaction) along with intraparticle diffusion controls the adsorption process steps and confirms the above-mentioned mechanisms.

## 4. Conclusions

The present study the adsorption of crystal violet in the batch system on magnetic chitosan nano-composites. This adsorbent was described following its characterization and identification by conventional techniques like Scanning Electron Microscopy, Particle-Size Distribution, X-Ray Diffraction, and Fourier Transform Infrared spectroscopy. Modelling and optimization of adsorption of cationic dyes from aqueous solutions by prepared nano-composite were studied using response surface methodology. The significance of the model was approved by analysis of variance (the coefficient of determination,  $R^2 = 0.75$ ,  $R^2_{\text{adj}} = 0.72$ ). A reduced second-order model was established as a functional relationship between four independent variables and the removal efficiency of the CV. Under optimum conditions (initial CV concentration = 77 mg/L, MCNCs dosage = 1 g/L, and contact time = 140 min) adsorption process led to a remarkable removal of CV (approximately 72%). Isotherm studies showed that the Freundlich model fitted the best the experimental data. According to the model, CV adsorption might be mainly a multi-molecular layer. The analysis of the adsorption rate at various contact times showed that dye adsorption followed the pseudo-first-order kinetic model. The endothermic enthalpy change of 123.91 kJ/mol and negative Gibbs free energy change

assured the spontaneous nature of the adsorption process. Based on the results of this study, it was concluded that the affordability, high potentiality, and well regenerability of MCNCs make it an attractive adsorbent in terms of wastewater remediation.

## Acknowledgements

This study is related to the project NO. 1396/64151 From Student Research Committee, Shahid Beheshti University of Medical Sciences, Tehran, Iran. We also appreciate the Student Research Committee and Research & Technology Chancellor in Shahid Beheshti University of Medical Sciences for their financial support of this study.

## Appendix A. Supplementary data

Supplementary material related to this article can be found, in the online version, at doi:<https://doi.org/10.1016/j.carbpol.2018.11.048>.

## References

- Ahmad, R., & Hasan, I. (2016). Optimization of the adsorption of Pb (II) from aqueous solution onto PAB nanocomposite using response surface methodology. *Environmental Nanotechnology, Monitoring & Management*, 6, 116–129.
- Ahmadi, M., Foladivanda, M., Jaafarzadeh, N., Ramezani, Z., Ramavandi, B., Jorfi, S., ... Kakavandi, B. (2017). Synthesis of chitosan zero-valent iron nanoparticles-supported for cadmium removal: Characterization, optimization and modeling approach. *Journal of Water Supply: Research and Technology-Aqua*, 66(2), 116–130.
- Ahmadi, M., Niari, M. H., & Kakavandi, B. (2017). Development of maghemite nanoparticles supported on cross-linked chitosan ( $\gamma$ -Fe<sub>2</sub>O<sub>3</sub>@CS) as a recoverable mesoporous magnetic composite for effective heavy metals removal. *Journal of Molecular Liquids*, 248, 184–196.
- Alimohammadi, M., Saedi, Z., Akbarpour, B., Rasoulzadeh, H., Yetilmezsoy, K., Al-Ghouti, M. A., Khraisheh, M., & McKay, G. (2017). Adsorptive removal of arsenic and mercury from aqueous solutions by eucalyptus leaves. *Water, Air, and Soil Pollution*, 228(11), 429.
- Asfaram, A., Ghaedi, M., Yousefi, F., & Dastkhooon, M. (2016). Experimental design and modeling of ultrasound assisted simultaneous adsorption of cationic dyes onto ZnS: Mn-NPs-AC from binary mixture. *Ultrasonics Sonochemistry*, 33, 77–89.
- Asfaram, A., Ghaedi, M., Hajati, S., Goudarzi, A., & Dil, E. A. (2017). Screening and optimization of highly effective ultrasound-assisted simultaneous adsorption of cationic dyes onto Mn-doped Fe<sub>3</sub>O<sub>4</sub>-nanoparticle-loaded activated carbon. *Ultrasonics Sonochemistry*, 34, 1–12.
- Ayazi, Z., Khoshhesab, Z. M., Azhar, F. F., & Mohajeri, Z. (2017). Modeling and optimization of adsorption removal of reactive orange 13 on the alginate–montmorillonite–polyaniline nanocomposite via response surface methodology. *Journal of the Chinese Chemical Society*, 64(6), 627–639.
- Bagheri, A. R., Ghaedi, M., Asfaram, A., Bazrafshan, A. A., & Jannesar, R. (2017). Comparative study on ultrasonic assisted adsorption of dyes from single system onto Fe<sub>3</sub>O<sub>4</sub> magnetite nanoparticles loaded on activated carbon: experimental design methodology. *Ultrasonics Sonochemistry*, 34, 294–304.
- Bandpei, A. M., Mohseni, S. M., Sheikhmohammadi, A., Sardar, M., Sarkhosh, M., Almasian, M., Avazpour, M., Mosallanejad, Z., Atafar, Z., & Nazari, S. (2017). Optimization of arsenite removal by adsorption onto organically modified montmorillonite clay: Experimental & theoretical approaches. *The Korean Journal of Chemical Engineering*, 34(2), 376–383.
- Cao, J., Luo, B., Lin, H., Xu, B., & Chen, S. (2012). Visible light photocatalytic activity enhancement and mechanism of AgBr/Ag<sub>3</sub>PO<sub>4</sub> hybrids for degradation of methyl orange. *Journal of Hazardous Materials*, 217, 107–115.
- Chang, Y.-C., & Chen, D.-H. (2005). Preparation and adsorption properties of mono-disperse chitosan-bound Fe<sub>3</sub>O<sub>4</sub> magnetic nanoparticles for removal of Cu (II) ions. *Journal of Colloid and Interface Science*, 283(2), 446–451.
- Chang, Q., Song, S., Wang, Y., Li, J., & Ma, J. (2012). Application of graphene as a sorbent for preconcentration and determination of trace amounts of chromium (III) in water samples by flame atomic absorption spectrometry. *Analytical Methods*, 4(4), 1110–1116.
- Dastkhooon, M., Ghaedi, M., Asfaram, A., Goudarzi, A., Mohammadi, S. M., & Wang, S. (2017). Improved adsorption performance of nanostructured composite by ultrasonic wave: Optimization through response surface methodology, isotherm and kinetic studies. *Ultrasonics Sonochemistry*, 37, 94–105.
- Dotto, G., Santos, J., Tanabe, E., Bertuol, D., Foletto, E., Lima, E., ... Pavan, F. (2017). Chitosan/polyamide nanofibers prepared by Forcspinning® technology: A new adsorbent to remove anionic dyes from aqueous solutions. *Journal of Cleaner Production*, 144, 120–129.
- Elwakeel, K. Z., El-Bindary, A., El-Sonbati, A., & Hawas, A. R. (2017a). Magnetic alginate beads with high basic dye removal potential and excellent regeneration ability. *Canadian Journal of Chemistry*(ja).
- Elwakeel, K. Z., El-Bindary, A., El-Sonbati, A., & Hawas, A. R. (2017b). Magnetic alginate beads with high basic dye removal potential and excellent regeneration ability. *Canadian Journal of Chemistry*, 95(8), 807–815.
- Ferreira, B. C. S., Teodoro, F. S., Mageste, A. B., Gil, L. F., de Freitas, R. P., & Gurgel, L. V. A. (2015). Application of a new carboxylate-functionalized sugarcane bagasse for adsorptive removal of crystal violet from aqueous solution: Kinetic, equilibrium and thermodynamic studies. *Industrial Crops and Products*, 65, 521–534.
- Geng, B., Jin, Z., Li, T., & Qi, X. (2009). Preparation of chitosan-stabilized Fe<sub>0</sub> nanoparticles for removal of hexavalent chromium in water. *The Science of the Total Environment*, 407(18), 4994–5000.
- Gupta, V. K., Agarwal, S., Asif, M., Fakhri, A., & Sadeghi, N. (2017). Application of response surface methodology to optimize the adsorption performance of a magnetic graphene oxide nanocomposite adsorbent for removal of methadone from the environment. *Journal of Colloid and Interface Science*, 497, 193–200.
- He, L., Yao, L., Liu, F., Qin, B., Song, R., & Huang, W. (2010). Magnetic Fe<sub>3</sub>O<sub>4</sub>@Chitosan Nanoparticle: Synthesis, Characterization and Application as Catalyst Carrier. *Journal of Nanoscience and Nanotechnology*, 10(10), 6348–6355.
- Jerold, M., Vasantharaj, K., Joseph, D., & Sivasubramanian, V. (2017). Fabrication of hybrid biosorbent nanoscale zero-valent iron-Sargassum swartzii biocomposite for the removal of crystal violet from aqueous solution. *International Journal of Phytoremediation*, 19(3), 214–224.
- Kurt, E., Koseoglu-Imer, D. Y., Dizge, N., Chellam, S., & Koyuncu, I. (2012). Pilot-scale evaluation of nanofiltration and reverse osmosis for process reuse of segregated textile dyewash wastewater. *Desalination*, 302, 24–32.
- Loqman, A., El Bali, B., Lützenkirchen, J., Weidler, P. G., & Kherbeche, A. (2016). Adsorptive removal of crystal violet dye by a local clay and process optimization by response surface methodology. *Applied Water Science*, 1–12.
- Makhado, E., Pandey, S., & Ramontja, J. (2018). Microwave assisted synthesis of xanthan gum-cl-poly (acrylic acid) based-reduced graphene oxide hydrogel composite for adsorption of methylene blue and methyl violet from aqueous solution. *International Journal of Biological Macromolecules*, 119, 255–269.
- Makhado, E., Pandey, S., Nomngongo, P. N., & Ramontja, J. (2018). Preparation and characterization of xanthan gum-cl-poly (acrylic acid)/o-MWCNTs hydrogel nanocomposite as highly effective re-usable adsorbent for removal of methylene blue from aqueous solutions. *Journal of Colloid and Interface Science*, 513, 700–714.
- Massoudinejad, M., Ghaderpoori, M., Shahsavani, A., & Amini, M. M. (2016). Adsorption of fluoride over a metal organic framework UiO-66 functionalized with amine groups and optimization with response surface methodology. *Journal of Molecular Liquids*, 221, 279–286.
- Massoudinejad, M., Ghaderpoori, M., Shahsavani, A., Jafari, A., Kamarehie, B., Ghaderpoori, A., ... Amini, M. M. (2018). Ethylenediamine-functionalized cubic ZIF-8 for arsenic adsorption from aqueous solution: Modeling, isotherms, kinetics and thermodynamics. *Journal of Molecular Liquids*, 255, 263–268.
- Mohammadzadeh, A., Ramezani, M., & Ghaedi, A. (2016). Synthesis and characterization of Fe<sub>2</sub>O<sub>3</sub>-ZnO-ZnFe<sub>2</sub>O<sub>4</sub>/carbon nanocomposite and its application to removal of bromophenol blue dye using ultrasonic assisted method: Optimization by response surface methodology and genetic algorithm. *Journal of the Taiwan Institute of Chemical Engineers*, 59, 275–284.
- Morshedi, D., Mohammadi, Z., Boojar, M. M. A., & Aliakbari, F. (2013). Using protein nanofibrils to remove azo dyes from aqueous solution by the coagulation process. *Colloids and Surfaces B, Biointerfaces*, 112, 245–254.
- Murugesan, A., Vidhyadevi, T., Kalaivani, S., Thiruvengadaravi, K., Ravikumar, L., Anuradha, C., ... Sivanesan, S. (2014). Modelling of lead (II) ion adsorption onto poly (thiourea imine) functionalized chelating resin using response surface methodology (RSM). *Journal of Water Process Engineering*, 3, 132–143.
- Muthukumar, C., Sivakumar, V. M., & Thirumarimurugan, M. (2016). Adsorption isotherms and kinetic studies of crystal violet dye removal from aqueous solution using surfactant modified magnetic nanoadsorbent. *Journal of the Taiwan Institute of Chemical Engineers*, 63, 354–362.
- Pandey, S. (2017). A comprehensive review on recent developments in bentonite-based materials used as adsorbents for wastewater treatment. *Journal of Molecular Liquids*, 241, 1091–1113.
- Pandey, S., & Mishra, S. B. (2014). Catalytic reduction of p-nitrophenol by using platinum nanoparticles stabilised by guar gum. *Carbohydrate Polymers*, 113, 525–531.
- Pandey, S., & Ramontja, J. (2016). Natural bentonite clay and its composites for dye removal: Current state and future potential. *American Journal of Chemistry and Applications*, 3(2), 8.
- Pei, Y., Wang, M., Tian, D., Xu, X., & Yuan, L. (2015). Synthesis of core-shell SiO<sub>2</sub>@MgO with flower like morphology for removal of crystal violet in water. *Journal of Colloid and Interface Science*, 453, 194–201.
- Podstawczyk, D., Witek-Krowiak, A., Dawiec, A., & Bhatnagar, A. (2015). Biosorption of copper (II) ions by flax meal: Empirical modeling and process optimization by response surface methodology (RSM) and artificial neural network (ANN) simulation. *Ecological Engineering*, 83, 364–379.
- Qian, F., Sun, X., & Liu, Y. (2013). Removal characteristics of organics in bio-treated textile wastewater reclamation by a stepwise coagulation and intermediate GAC/O<sub>3</sub> oxidation process. *Chemical Engineering Journal*, 214, 112–118.
- Rafatullah, M., Sulaiman, O., Hashim, R., & Ahmad, A. (2010). Adsorption of methylene blue on low-cost adsorbents: A review. *Journal of Hazardous Materials*, 177(1), 70–80.
- Rai, P., Gautam, R. K., Banerjee, S., Rawat, V., & Chattopadhyaya, M. (2015). Synthesis and characterization of a novel SnFe<sub>2</sub>O<sub>4</sub>@activated carbon magnetic nanocomposite and its effectiveness in the removal of crystal violet from aqueous solution. *Journal of Environmental Chemical Engineering*, 3(4), 2281–2291.
- Reddy, D. H. K., & Lee, S.-M. (2013). Application of magnetic chitosan composites for the removal of toxic metal and dyes from aqueous solutions. *Advances in Colloid and Interface Science*, 201, 68–93.
- Saad, M., Tahir, H., Khan, J., Hameed, U., & Saud, A. (2017). Synthesis of polyaniline nanoparticles and their application for the removal of Crystal Violet dye by ultrasonic adsorption process based on Response Surface Methodology. *Ultrasonics Sonochemistry*, 34, 600–608.

- Saleh, T. A., Sari, A., & Tuzen, M. (2017). Effective adsorption of antimony (III) from aqueous solutions by polyamide-graphene composite as a novel adsorbent. *Chemical Engineering Journal*, 307, 230–238.
- Sarma, G. K., Gupta, S. S., & Bhattacharyya, K. G. (2016). Adsorption of Crystal violet on raw and acid-treated montmorillonite, K10, in aqueous suspension. *Journal of Environmental Management*, 171, 1–10.
- Sohbatzadeh, H., Keshtkar, A. R., Safdari, J., & Fatemi, F. (2016). U (VI) biosorption by bi-functionalized *Pseudomonas putida* chitosan bead: Modeling and optimization using RSM. *International Journal of Biological Macromolecules*, 89, 647–658.
- Subramaniam, R., & Ponnusamy, S. K. (2015). Novel adsorbent from agricultural waste (cashew NUT shell) for methylene blue dye removal: Optimization by response surface methodology. *Water Resources and Industry*, 11, 64–70.
- Tahir, N., Bhatti, H. N., Iqbal, M., & Noreen, S. (2017). Biopolymers composites with peanut hull waste biomass and application for Crystal Violet adsorption. *International Journal of Biological Macromolecules*, 94, 210–220.
- Vakili, M., Rafatullah, M., Salamatinia, B., Abdullah, A. Z., Ibrahim, M. H., Tan, K. B., Gholami, Z., & Amouzgar, P. (2014). Application of chitosan and its derivatives as adsorbents for dye removal from water and wastewater: A review. *Carbohydrate Polymers*, 113, 115–130.
- Van Thuan, T., Quynh, B. T. P., Nguyen, T. D., & Bach, L. G. (2017a). Response surface methodology approach for optimization of Cu<sup>2+</sup>, Ni<sup>2+</sup> and Pb<sup>2+</sup> adsorption using KOH-activated carbon from banana peel. *Surfaces and Interfaces*, 6, 209–217.
- Van Thuan, T., Quynh, B. T. P., Nguyen, T. D., & Bach, L. G. (2017b). Response surface methodology approach for optimization of Cu<sup>2+</sup>, Ni<sup>2+</sup> and Pb<sup>2+</sup> adsorption using KOH-activated carbon from banana peel. *Surfaces and Interfaces*, 6, 209–217.
- Van Tran, T., Bui, Q. T. P., Nguyen, T. D., & Bach, L. G. (2017c). Application of response surface methodology to optimize the fabrication of ZnCl<sub>2</sub>-activated carbon from sugarcane bagasse for the removal of Cu<sup>2+</sup>. *Water Science & Technology*, 75(9), 2047–2055.
- Yilmaz, Ş., Şahan, T., & Karabakan, A. (2017). Response surface approach for optimization of Hg (II) adsorption by 3-mercaptopropyl trimethoxysilane-modified kaolin minerals from aqueous solution. *The Korean Journal of Chemical Engineering*, 1–11.
- Yu, C., Geng, J., Zhuang, Y., Zhao, J., Chu, L., Luo, X., Zhao, Y., & Guo, Y. (2016). Preparation of the chitosan grafted poly (quaternary ammonium)/Fe<sub>3</sub>O<sub>4</sub> nanoparticles and its adsorption performance for food yellow 3. *Carbohydrate Polymers*, 152, 327–336.
- Zhou, Y., Zhang, M., Wang, X., Huang, Q., Min, Y., Ma, T., ... Niu, J. (2014). Removal of crystal violet by a novel cellulose-based adsorbent: Comparison with native cellulose. *Industrial & Engineering Chemistry Research*, 53(13), 5498–5506.
- Zulfikar, M. A., Afrita, S., Wahyuningrum, D., & Ledyastuti, M. (2016a). Preparation of Fe<sub>3</sub>O<sub>4</sub>-chitosan hybrid nano-particles used for humic acid adsorption. *Environmental Nanotechnology, Monitoring and Management*, 6, 64–75.
- Zulfikar, M. A., Afrita, S., Wahyuningrum, D., & Ledyastuti, M. (2016b). Preparation of Fe<sub>3</sub>O<sub>4</sub>-chitosan hybrid nano-particles used for humic acid adsorption. *Environmental Nanotechnology, Measuring Monitoring Management Control*, 6, 64–75.
- Zulfikar, M. A., Afrita, S., Wahyuningrum, D., & Ledyastuti, M. (2016c). Preparation of Fe<sub>3</sub>O<sub>4</sub>-chitosan hybrid nano-particles used for humic acid adsorption. *Environmental Nanotechnology, Measuring Monitoring Management Control*, 6, 64–75.